X-RAY, RADIO, AND OPTICAL OBSERVATIONS OF CASSIOPEIA A

T. DeLaney

University of Minnesota

116 Church St. SE, Minneapolis, MN 55455, U.S.A.

TDELANEY@ASTRO.UMN.EDU

L. Rudnick, T. W. Jones, R. Fesen, U. Hwang, R. Petre, J. Morse

LARRY@ASTRO.UMN.EDU, TWJ@ASTRO.UMN.EDU, FESEN@SNR.DARTMOUTH.EDU

HWANG@ORFEO.GSFC.NASA.GOV, PETRE@LHEAVX.GSFC.NASA.GOV, JON.MORSE@ASU.EDU

Abstract

We have performed a multi-wavelength comparison of Cassiopeia A using Very Large Array, *Hubble* Space Telescope, and *Chandra* X-ray Observatory images. By separating components spectrally, we find clear associations between the emission at the three wavebands. We separate the emitting material into two components – shocked circumstellar medium (CSM) and shocked ejecta, which show the same respective morphologies and proper motions in the different bands. In the shocked CSM, we find matched low-energy enhanced X-ray emission and optical quasi-stationary flocculi, and X-ray continuum-dominated emission matched with filamentary radio structures. In the shocked ejecta, we find matched silicon and iron dominated X-ray emission and optical fast-moving knots.

1 Introduction

Cassiopeia A (Cas A) is one of the brightest X-ray and radio sources in the sky. It is the youngest known ($\sim$ 330 per year, Thorstensen, Fesen & van den Bergh, 2001) Galactic supernova remnant (SNR) and is about 3.4 kpc away (Reed et al., 1995). It was most likely the result of either a type Ib or IIn supernova explosion (Chevalier & Oishi, 2003). At radio, X-ray, and optical wavelengths (see Fig. 1), Cas A consists of a $3'.5$ diameter bright ring of emission with a fainter X-ray and radio plateau extending to $\sim 5'$. The X-ray emission is dominated by a thermal spectrum consistent with highly ionized ejecta. The radio emission results from synchrotron radiation from electrons. The optical emission results from chemically enriched ejecta and circumstellar media (CSM).

The mean rate of expansion of the radio knots is 0.11% yr^{-1} with variations of up to a factor of two as a function of azimuth (Anderson & Rudnick, 1995; Koralesky et al., 1998; Tuffs, 1986). The radio knots have been significantly decelerated relative to the X-ray and optical emission and are not in homologous expansion – some even show inward motions. The optical emission in Cas A arises from slow-moving ($\lesssim 500$ km s^{-1}) quasi-stationary flocculi (QSFs) and fast moving knots (FMKs, 4000–6000 km s^{-1}, $\sim 0.3\%$ yr^{-1}, Kamper & van den Bergh, 1976; van den Bergh & Kamper, 1985). The QSFs are thought to be shocked CSM from the wind of the progenitor while most of the FMKs are located on the bright ring and represent emission from ejecta. There are also outlying knots with velocities from 8000–15,000 km s^{-1} ($\sim 0.3\%$ yr^{-1}, Fesen, 2001).

Previous X-ray proper motion measurements, conducted with *EINSTEIN* and *ROSAT* at a resolution of $5''$, showed that the mean expansion rate was 0.2% yr^{-1} (Koralesky et al., 1998; Vink et al., 1998). This established a difference in expansion rates for the co-spatial bright ring of approximately 3:2:1 for the optical, X-ray, and radio, respectively (Thorstensen, Fesen & van den Bergh, 2001, and references therein). The factor of two discrepancy between the X-ray and radio expansion has also been found in both Kepler's SNR (Hughes, 1999; Dickel et al., 1988) and Tycho's SNR (Hughes, 2000).

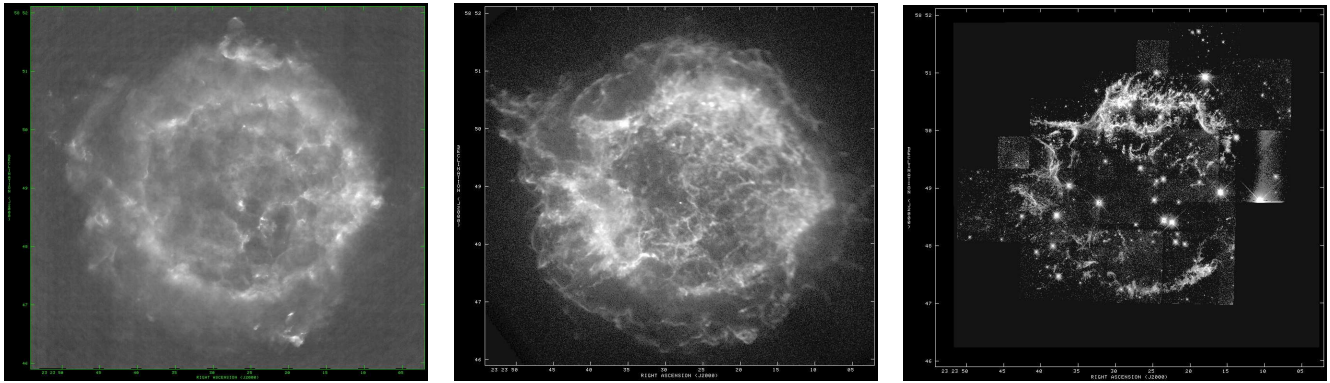With the advent of *Chandra*, we are now able to measure proper motions with unprecedented spatial res-

Figure 1: Left: Radio 6cm VLA image, Center: *Chandra* 0.3–10keV X-ray image (square root intensity scale), Right: *HST* optical image showing primarily the emission lines of [S II], [O II], [O I], and [N II] (square root intensity scale).

olution. The results for the forward shock filaments around the outer edge of the remnant showed a mean expansion rate of 0.21% yr^{-1} (DeLaney & Rudnick, 2003), the same as the bright ring. In this paper we extend the X-ray proper motion analysis to the rest of the SNR, identify spectrally distinct X-ray components with radio and optical counterparts, and interpret the proper motions based on these spectral components.

2 Distinct X-ray spectral components

The X-ray emission can be classified into four major spectrally distinct components: Si-dominated, Fe-dominated, low energy (LowE) enhanced, and continuum-dominated. The Si-, Fe-, and continuum-dominated classes were previously identified by Hughes et al. (2000). Representative spectra are shown in Fig. 2. The Si-dominated emission has very strong line emission from Si and S as well as O, Ca, Ar, and Mg. The Fe-dominated spectrum has strong Fe L and Fe K emission and may in some cases have almost pure Fe emission (Hwang & Laming, 2003; Laming & Hwang, 2003). The LowE-enhanced emission shows a relative increase in emission at low energies (~ 0.8–1.6 keV) compared to the global spectrum. The continuum-dominated emission shows little or no line emission and an increase in 4–6 keV emission relative to the global spectrum.

To spatially visualize the spectral components, we used spectral tomography. The spectral tomography technique involves taking differences between images from two different energies with a scale factor chosen to accentuate features of interest. In Fig. 3 we show four tomography images each representing the dominant spectral type indicated by the spectra in Fig. 2. For

details related to the tomography image construction, see DeLaney et al. (2004).

The Si-dominated and Fe-dominated tomography images basically reproduce the spatial distributions of Si and Fe as shown by the equivalent width images in Hwang, Holt & Petre (2000). However, there is significant absorption of low energy X-ray emission to the west (Keohane, Rudnick & Anderson, 1996; Willingale et al., 2002) making it difficult to properly represent the actual Si and Fe emission present there. The continuum-dominated image highlights the forward shock filaments around the outer edge of the remnant as described by Gotthelf et al. (2001) and also shows filamentary emission across the face of the remnant. Hughes et al. (2000) speculated that the apparent interior continuum-dominated filaments result from X-ray synchrotron emission associated with the forward shock. The continuum-dominated image matches the 8–15 keV *XMM-Newton* continuum image (Bleeker et al., 2001), especially in the west, indicating that there may be a strong non-thermal component to the continuum-dominated X-ray emission. The LowE-enhanced image represents a newly identified component of the X-ray emission. In addition to emission in the interior of the remnant, a southern arc is clearly visible.

3 X-ray proper motions

High resolution X-ray proper motions were measured between the 2000 and 2002 *Chandra* images as described in DeLaney et al. (2004). Histograms showing the radial expansion rates broken down by spectral class are shown in Fig. 4. Also included for completeness are the expansion rates from the twenty-nine for-
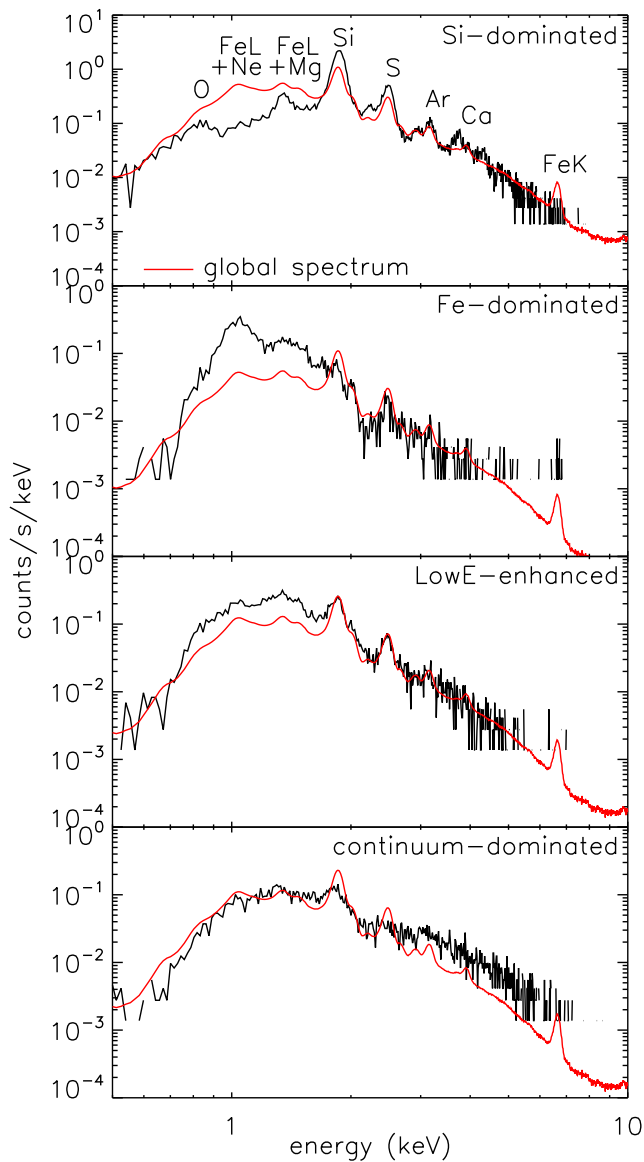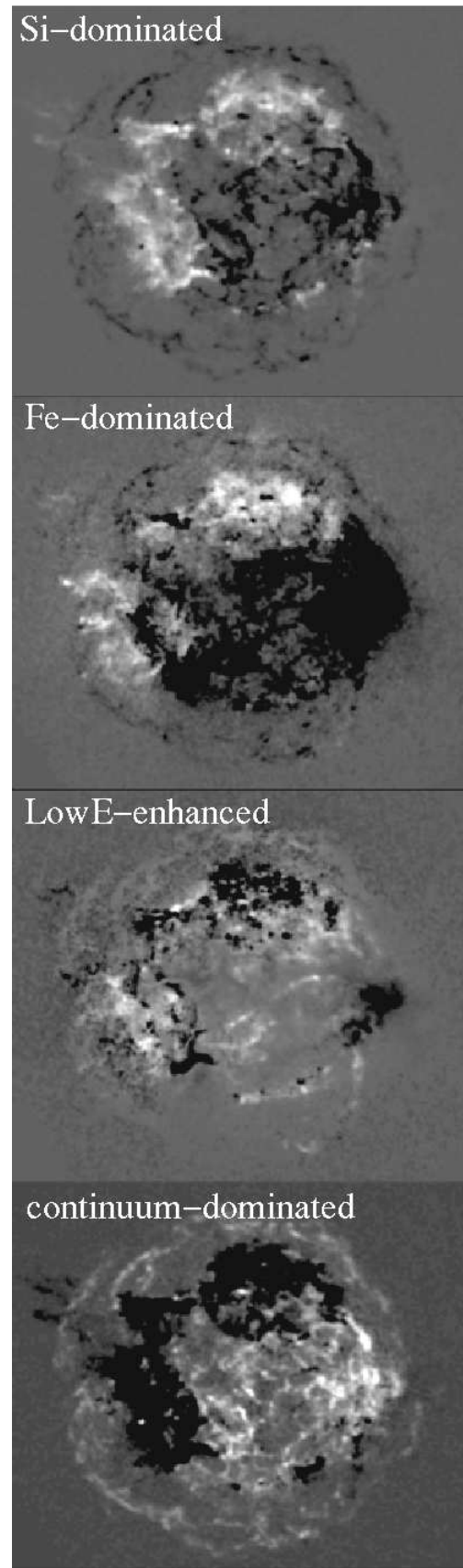
Figure 2: *Chandra* ACIS-S spectra of Cas A showing the global spectrum and typical spectra for the four spectral classes identified in the text.

Figure 3: Right: Representative tomography images used to spatially identify emission from the four classes whose spectra are shown in Fig. 2.

ward shock filaments presented in DeLaney & Rudnick (2003). Although the expansion rate distribution of the knots and filaments is very broad, when broken down by spectral class, it is clear that each species has its own characteristic expansion rate.

The Si- and Fe-dominated ejecta knots have the fastest expansion rates with a mean value of $0.2\pm0.01\%$ yr^{-1}. This does not mean that the two populations have the
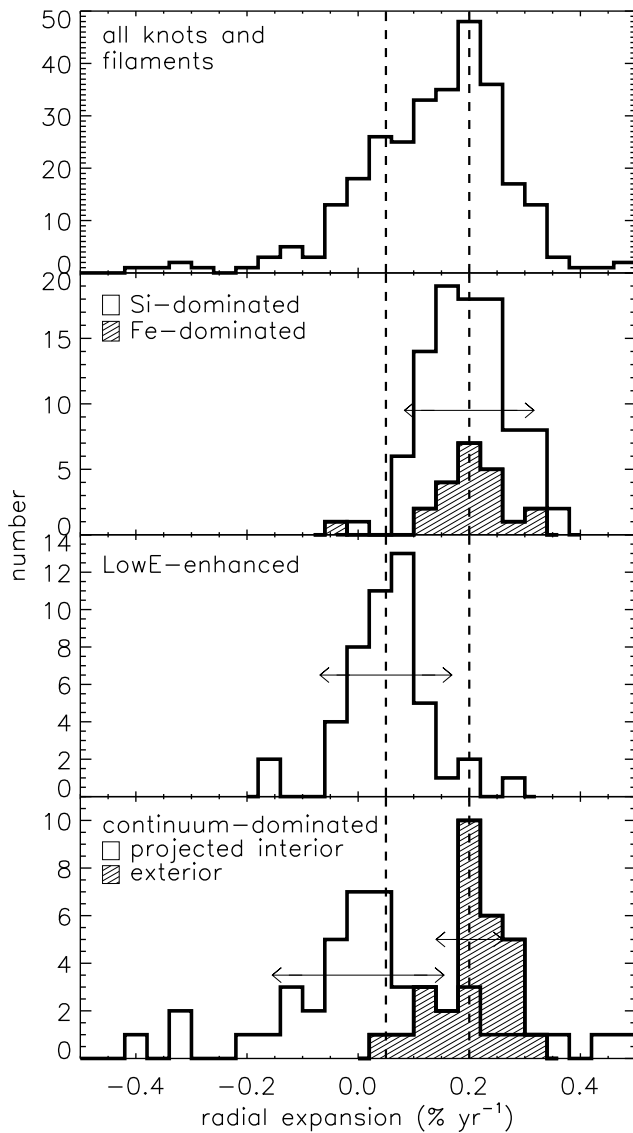
Figure 4: Histograms of X-ray expansion rates in Cas A broken down by spectral class. Arrows show the average measurement error for each population. Dashed lines mark the mean expansion rates for the Si-dominated and LowE-enhanced populations. The free expansion rate is 0.3% yr^{-1}. The "exterior" continuum-dominated filaments are from DeLaney & Rudnick (2003).
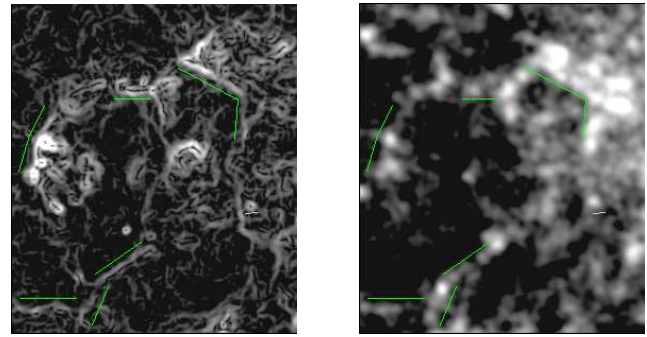

Figure 5: Radio emission filtered to enhance edges (left) and continuum-dominated X-ray emission (right) for a region west and south of the center of Cas A. There are significant correlations between the radio emission and the continuum-dominated X-ray emission as shown by the green lines.
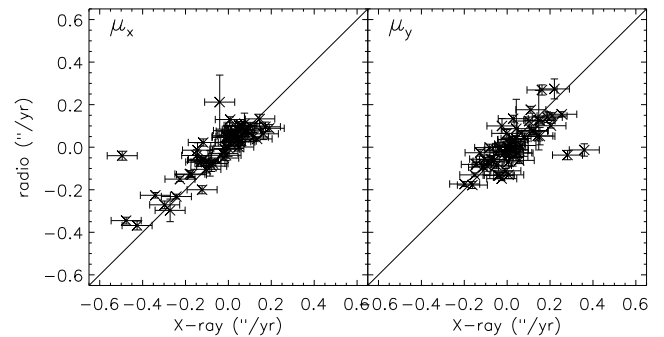

Figure 6: Scatter plots showing the proper motions (left: μ_x, right: μ_y) for *all* spatially matched X-ray and radio knots including both continuum-dominated and ejecta X-ray knots.

same average velocity. The Si-dominated knots are at an average radius of $95''$ which converts to a velocity of 3100 km s^{-1} for a distance of 3.4 kpc to Cas A. The Fe-dominated knots lie further out on average at a radius of $120''$ yielding an average velocity of 3900 km s^{-1} for the same expansion rate. These velocities are faster than the Doppler velocities of 2000–3000 km s^{-1} for the *Chandra* Si emission (Hwang et al., 2001), ~ 1000 km s^{-1} for the *XMM-Newton* Si and S

emission, and ~ 1500 km s^{-1} for the *XMM-Newton* Fe K emission (Willingale et al., 2002). The slightly faster Fe Doppler velocity compared to Si and S agrees with our result that the Fe knots have a higher velocity than the Si knots. The mismatch of Doppler velocities and expansion rates is not surprising since they would match only if the ejecta were uniformly distributed, which is not the case (Willingale et al., 2002).

The continuum-dominated knots and filaments are classified as "exterior" and "projected interior" where the exterior features are the forward shock filaments around the edge of the remnant. The exterior features have a mean expansion rate of 0.2±0.01% yr^{-1} while the projected interior features have more chaotic behavior with large variations in expansion rate and apparent inward motions. Most of the inward motions are concentrated to the south and west between 170° and 300° azimuth where the radio proper motion mea-
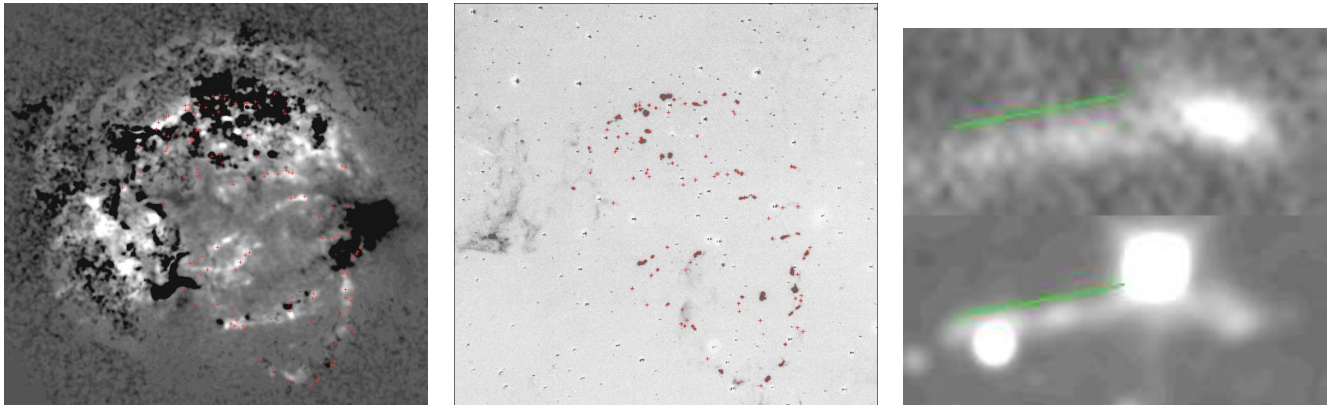
Figure 7: Left: LowE-enhanced X-ray image with red crosses marking the positions of QSF knots identified in the continuum-subtracted Hα image (center, adapted from Fesen (2001)). Right: close up of one such matched QSF (bottom) and X-ray knot (top) near α(J2000) = $23^{\mathrm{h}}23^{\mathrm{m}}19^{\mathrm{s}}$, δ(J2000) = $58°49'3''8$.

surements also show inward moving features (Anderson & Rudnick, 1995). The LowE-enhanced knots are moving quite slowly with a mean expansion rate of $0.05\pm0.01\%$ yr^{-1}.

4   Radio and continuum-dominated X-rays

Just as the forward shock filaments identified by Gotthelf et al. (2001) are associated with the edge of the radio plateau, the continuum-dominated filaments across the face of the remnant are associated with edges and filaments of radio emission as shown in Fig. 5. Furthermore, where X-ray and radio features match, the proper motions match as well as shown in Fig. 6. The interior continuum-dominated filaments have the same X-ray spectral shape as the exterior forward shock filaments and both are associated with steep radio spectral index features (Anderson & Rudnick, 1996). Based on these similarities, we propose that the interior continuum-dominated filaments are projected forward shock filaments.

The projected interior filaments are not evenly distributed across the face of the remnant, but rather are concentrated to the west where there is significant X-ray absorption (Keohane, Rudnick & Anderson, 1996; Willingale et al., 2002). The "inward" motions and the motions seemingly faster than free expansion are consistent with the forward shock illuminating the CSM as it expands into and interacts with the clumpy, nonuniform environment. When seen face on, the forward shock motions appear chaotic. We may also be observing a more complex pattern which includes both motions and changes in synchrotron brightness as CSM

clumps are enveloped by the forward shock causing magnetic field amplification in shear layers and turbulent wakes (Jones & Kang, 1993).

The interior continuum-dominated filaments have also been interpreted as non-thermal bremsstrahlung emission associated with the ejecta/reverse shock (Bleeker et al., 2001). The *XMM-Newton* hard X-ray continuum images show that the emission in the west is much brighter than the forward shock filaments which may indicate that the two continuum-dominated populations have different emission processes. If the interior filaments are internal to the SNR, they are unlikely to have significant X-ray synchrotron emission because the high magnetic filed strength will cause rapid aging of electrons at X-ray energies (Vink & Laming, 2003).

5   Optical QSFs and LowE-enhanced X-rays

Spatially, many of the LowE-enhanced X-ray features match very well with optical QSF emission, particularly the arc to the south, the emission just to the exterior of the bright ring to the northeast, and much of the interior emission as shown in Fig. 7. Where QSF and LowE-enhanced features match, the proper motions also match as shown in Fig. 8. Based on the spatial and dynamical similarities, we propose that the LowE-enhanced X-ray emission, like the optical QSF emission, represents the clumpy component of the CSM that was deposited by the wind from the massive progenitor.

Despite the fact that matched features show the same proper motions, on average, QSFs show little or no motion (van den Bergh & Kamper, 1985) while the
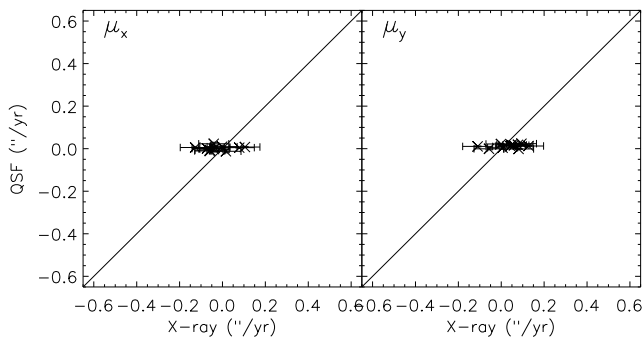
Figure 8: Scatter plots showing the proper motions (left: μ_x, right: μ_y) for spatially matched X-ray and optical QSF knots.

Figure 9: Scatter plots showing the proper motions (left: μ_x, right: μ_y) for spatially matched X-ray and optical FMK knots.

mean expansion rate of the LowE-enhanced knots is $0.05\pm0.01\%$ yr^{-1}. The difference in expansion rates between the optical QSF population and the X-ray LowE-enhanced population might be due to a pre-existing density distribution in the progenitor wind (Chevalier & Oishi, 2003). On average, less dense X-ray clumps may be accelerated more by the forward shock than more dense optical clumps. A softer X-ray spectrum is expected as slow shocks propagate through dense clumps producing a spectrum with a cooler characteristic temperature (Hester & Cox, 1986; Park et al., 2003).

There is also LowE-enhanced emission which has no QSF counterparts such as in the southeast. This may be because the low energy spectral region contains emission lines of O, Fe, Ne, and Mg, making it is possible that some of the emission in the LowE-enhanced image is due to more than one spectral component.

6   Ejecta emission

Our new, high-resolution proper motion measurements show that the X-ray ejecta are moving slower on average than the co-spatial optical ejecta and faster on average than the co-spatial radio knots as was observed previously with *EINSTEIN* and *ROSAT* (Koralesky et al., 1998; Vink et al., 1998). There are a small number of matched X-ray/optical and matched X-ray/radio knots which have the same motions as shown in Fig. 9 and Fig. 6, respectively. The X-ray/optical population difference is thought to be due to the density difference between the two populations (Anderson et al., 1994; Hwang et al., 2001; Fesen, 2001; DeLaney & Rudnick, 2003). High density ejecta are not very decelerated and thus are not significantly disrupted, allowing the
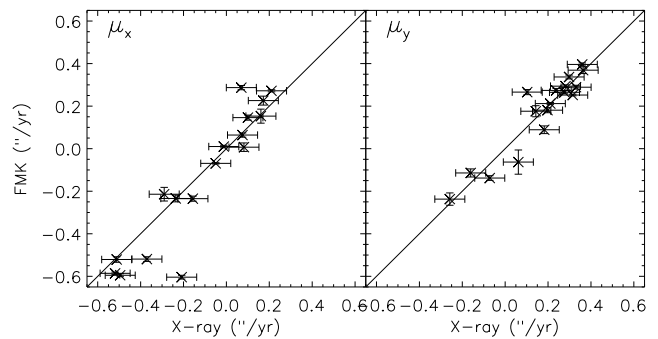
ejecta to cool rather quickly and emit at optical wavelengths. Low density ejecta experience more deceleration, and are heated to higher temperatures. These ejecta emit at X-ray wavelengths and may experience significant disruption before they can cool to optically emitting temperatures. The radio emission arises from synchrotron radiation, which requires amplification of magnetic fields to be strong enough for the emission to be seen. This amplification likely results from the turbulence associated with the deceleration of the ejecta. If significant deceleration is needed for amplification, radio emitting knots would be decelerated the most.

Of particular interest is the fact that the Si- and Fe-dominated ejecta have experienced the same apparent fractional deceleration in their expansion rate (from free expansion at 0.3% yr^{-1} to 0.2% yr^{-1}). The Fe-rich emission (which results from explosive silicon burning near the core of the progenitor) is on average exterior to the Si-group emission (which results from explosive oxygen burning farther out from the star's center). This spatial separation might arise from either a difference in the initial ejection velocities or from a difference in deceleration after interaction with the reverse shock. In either case, one would not necessarily expect the Si and Fe to have been decelerated by the same fractional amount. Furthermore, the X-ray ejecta have the same expansion rate as the forward shock filaments (i.e., homologous expansion on average), perhaps implying that the two populations are part of a coupled dynamical system in which the pressure in the X-ray ejecta is determined by the forward shock speed; although this does not explain why the optical ejecta would not be affected. Even if initially the ejecta were not coupled to the forward shock speed, after interaction with the reverse shock and secondary shocks, the

ejecta may now be expanding with the forward shock (Laming & Hwang, 2003).

7   Conclusion

In summary, both the high-resolution X-ray proper motion measurements and the X-ray spectral classes, show that the X-ray emission can be separated into shocked CSM and shocked ejecta. The shocked CSM can be further separated into a clumpy and a diffuse component. Each component has a distinct kinematic signature. The ejecta component consists of both Si- and Fe-dominated emission populations, is associated with optical FMK emission, and has experienced significant decelerated relative to the FMKs. The greater deceleration of the X-ray ejecta on average compared to the optical ejecta is due to the relatively lower densities in the X-ray material. The clumpy CSM component consists of slow-moving LowE-enhanced emission and is analogous to optical QSF emission. The diffuse CSM may be associated with continuum-dominated emission from material swept up by the forward shock. The projected interior continuum-dominated filaments have chaotic motions which may be explained by an interaction with the absorbing CSM in that region. The X-ray ejecta has the same expansion rate as the exterior forward shock filaments suggesting a dynamic coupling between the forward shock and the ejecta.

Acknowledgments

References

Anderson, M., Jones, T. W., Rudnick, L., Tregillis, I. L., Kang, H. 1994, ApJ, 421, L31

Anderson, M., Rudnick, L. 1995, ApJ, 441, 307

Anderson, M., Rudnick, L. 1996, ApJ, 456, 234

Bleeker, J. A. M., Willingale, R., van der Heyden, K., Dennerl, K., Kaastra, J. S., Aschenbach, B., Vink, J. 2001, MNRAS, 365, L225

Chevalier, R., Oishi, J. 2003, ApJ, 593, L23

DeLaney, T., Rudnick, L. 2003, ApJ, 589, 818

DeLaney, T., Rudnick, L., Fesen, R., Jones, T. W., Petre, R., Morse, J. 2004, ApJ, submitted

Dickel, J. R., Sault, R., Arendt, R. G., Matsui, Y., Korista, K. T. 1988, ApJ, 330, 254

Fesen, R. A. 2001, ApJS, 133, 161

Gotthelf, E., Koralesky, B., Rudnick, L., Jones, T., Hwang, U., Petre, R. 2001, ApJ, 552, L39

Hester, J. J., Cox, D. P. 1986, ApJ, 300, 675

Hughes, J. P. 1999, ApJ, 527, 298

Hughes, J. P. 2000, ApJ, 545, L53

Hughes, J. P., Rakowski, C. E., Burrows, D. N., Slane, P. O. 2000, ApJ, 528, L109

Hwang, U., Holt, S., Petre, R. 2000, ApJ, 537, L119

Hwang, U., Laming, J. M. 2003, ApJ, 597, 362

Hwang, U., Szymkowiak, A. E., Petre, R., Holt, S. S. 2001, ApJ, 560, L175

Jones, T. W., Kang, H. 1993, ApJ, 402, 560

Kamper, K., van den Bergh, S. 1976, ApJS, 32, 351

Keohane, J. W., Rudnick, L., Anderson, M. C. 1996, ApJ, 466, 309

Koralesky, B., Rudnick, L., Gotthelf, E., Keohane, J. 1998, ApJ, 505, L27

Laming, J. M., Hwang, U. 2003, ApJ, 597, 347

Park, S., Burrows, D. N., Garmire, G. P., Nousek, J. A., Hughes, J. P., Williams, R. M. 2003, ApJ, 586, 210

Reed, J. E., Hester, J. J., Fabian, A. C., Winkler, P. F. 1995, ApJ, 440, 706

Thorstensen, J., Fesen, R., van den Bergh, S. 2001, AJ, 122, 297

Tuffs, R. 1986, MNRAS, 219, 13

van den Bergh, S., Kamper, K. 1985, ApJ, 293, 537

Vink, J., Bloemen, H., Kaastra, J. S., Bleeker, J. A. M. 1998, A&A, 339, 201

Vink, J., Laming, J. M. 2003, ApJ, 584, 758

Willingale, R., Bleeker, J. A. M., van der Heyden, K. J., Kaastra, J. S., Vink, J. 2002, A&A, 381, 1039